Peptide stereocomplexation orchestrates supramolecular assembly of hydrogel biomaterials

Israt Jahan Duti[1], Jonathan R. Florian[2], Anna R. Kittel[2], Connor D. Amelung[2], Vincent P. Gray[1], Kyle J. Lampe[1]*, Rachel A. Letteri[1]*.

[1]Department of Chemical Engineering, University of Virginia, Charlottesville VA 22903

[2]Department of Biomedical Engineering, University of Virginia, Charlottesville VA 22903

ABSTRACT: Stereocomplexation, or stereochemistry-directed interactions among complementary stereoregular macromolecules, is burgeoning as an increasingly impactful design tool, exerting exquisite control of material structure and properties. Since stereocomplexation of polymers produces remarkable transformations in mechanics, morphology, and degradation, we sought to leverage stereocomplexation to tune these properties in peptide-based biomaterials. We found that blending the pentapeptides L- and D-KYFIL triggers dual mechanical and morphological transformations from stiff fibrous hydrogels into less stiff networks of plates, starkly contrasting prior reports of blending L- and D-peptides producing stiffer fibrous hydrogels than the individual constituents. The morphological transformation of KYFIL in phosphate-buffered saline, from fibers that entangle into hydrogels to plates that cannot entangle, explains the accompanying mechanical transformation. Moreover, the blends shield L-KYFIL from proteolytic degradation, producing materials with comparable proteolytic stability to D-KYFIL but with distinct 2D plate morphologies that in biomaterials may promote unique therapeutic release profiles and cell behavior. To confirm that these morphological, mechanical, and stability changes arise from differences in molecular packing as in polymer stereocomplexation, we acquired x-ray diffraction patterns, which showed L- and D-KYFIL to be amorphous and their blends crystalline. Stereocomplexation is particularly apparent in pure water, where L- and D-KYFIL are soluble random coils and their blends form β-sheets and gel within minutes. Collectively, these results highlight the role of molecular details, such as peptide sequence, in determining the material properties resulting from stereocomplexation. Looking forward, the ability of stereocomplexation to orchestrate supramolecular assembly and tune application-critical properties champions stereochemistry as a compelling design consideration.

INTRODUCTION

Designer biomaterials emulating the mechanical, chemical, and topological features of native tissue[1–5] can direct cell behavior, enabling in vitro tissue models[6–11] and in vivo tissue regeneration[12–15]. Exhibiting tunable, tissue-mimetic viscoelasticity and morphology, supramolecularly assembling peptides are ideal building blocks for such designer biomaterials[4,16–20]. Peptide sequence modulates molecular scale interactions (electrostatic, pi-pi stacking, hydrogen bonding, and hydrophobic) that determine the macroscale mechanics, morphology, and stability of biomaterials[21,22]. Here, we sought to enrich the molecular engineering toolkit for peptide-based biomaterials by invoking and understanding the role of peptide stereochemistry in tuning molecular scale interactions and bulk biomaterial properties.

Specific interactions between complementary stereoregular macromolecules are known in the synthetic polymer literature as stereocomplexation. By directing molecular packing, stereocomplexation leads to thermomechanical properties, morphologies, and material lifetimes distinct from those of the individual components[23–34]. For example, poly(L-lactic acid) (PLLA) and poly(D-lactic acid) (PDLA) melt at 170–180 °C, while their 1:1 stereocomplex blends melt nearly 50 ºC higher at 220–230 °C[24,25]. Furthermore, the half-life of PLLA heptamers in aqueous buffer at 37 ºC is only 1 h, whereas that of PLLA/PDLA stereocomplexes is 3.5 days[32]. These alterations in materials properties upon stereocomplexation of poly(lactic acid) and a variety of other stereoregular polymers result from different molecular packing arrangements typically probed with x-ray scattering[26,29,30]. Since stereocomplexation capably controls material mechanics, morphology, and lifetime, these interactions have tremendous potential as building blocks of designer biomaterials.

Like poly(lactic acid), peptides have complementary L- and D-isomers that can interact specifically to generate biomaterials with properties distinct from their constituents. For instance, both the L- and D-forms of the β-sheet peptide 'MAX1' assemble into 3D fibrous hydrogels with storage shear moduli (G') of ~ 200 Pa. Blending the L- and D-peptides at a 1:1 ratio yields stiffer hydrogels, with G' ~ 800 Pa[35–37]. In addition to changing mechanics, blends of L- and D-peptides bolster the proteolytic stability of L-peptides, the predominant stereochemical configuration of natural peptides and proteins. Upon incubation with protease, the L-form of the amphipathic β-sheet peptide Ac-$(FKFE)_2$-NH_2 degrades within 1 day. In contrast, 1:1 blends of L- and D-$(FKFE)_2$ remain stable for at least 5 days, similar to the protease-resistant D-form[37–39]. With respect to morphology, the 1:1 blends of MAX1 and Ac-$(FKFE)_2$-NH_2 retain the nanoscale fibrous morphology of their L- and D-peptide constituents. In contrast, blending L- and D-forms of the amyloid-β peptide Aβ(16-22) triggers a morphological transformation from nanoscale fibers to micron-scale needlelike structures[37,40]. Therefore, upon introducing new L- and D-peptides as

components of assembling biomaterials, we will need to understand the impacts of stereochemistry-directed assembly on mechanics, morphology, and stability.

In this work, we investigate how stereochemistry-directed assembly of peptides or '*peptide stereocomplexation*' tunes the molecular-level and bulk properties of biomaterials formed from a class of supramolecularly assembling peptides termed rapidly assembling pentapeptides for injectable delivery (RAPID). RAPID peptides are promising building blocks of biomaterials for tissue engineering and regenerative medicine, as they assemble in 1X phosphate buffered saline (PBS) at pH 7.4 into fibrous hydrogels that mimic a range of native tissue stiffnesses[41,42]. These hydrogels shear-thin, self-heal, and protect neural cells from membrane-damaging extensional flow during needle extrusion[42]. Here, we study the stereocomplexation of the RAPID peptide KYFIL to highlight and provide guidance for the use of stereocomplexation as a molecular design tool in tuning peptide-based biomaterials to mimic native tissue.

RESULTS AND DISCUSSION

To gain insight into how peptide stereocomplexation orchestrates assembly and determines the molecular-level, nanoscale, and bulk properties of KYFIL biomaterials, we measure solution turbidity, secondary structure, X-ray diffraction patterns, mechanics, morphology, and proteolytic stability as a function of stereochemical composition (i.e., the ratio of L-KYFIL: D-KYFIL). We initially provide evidence for KYFIL stereocomplexation in water and then proceed to study stereocomplexation in solutions with physiological salt and pH that promote self-assembly of L- and D-KYFIL peptides.

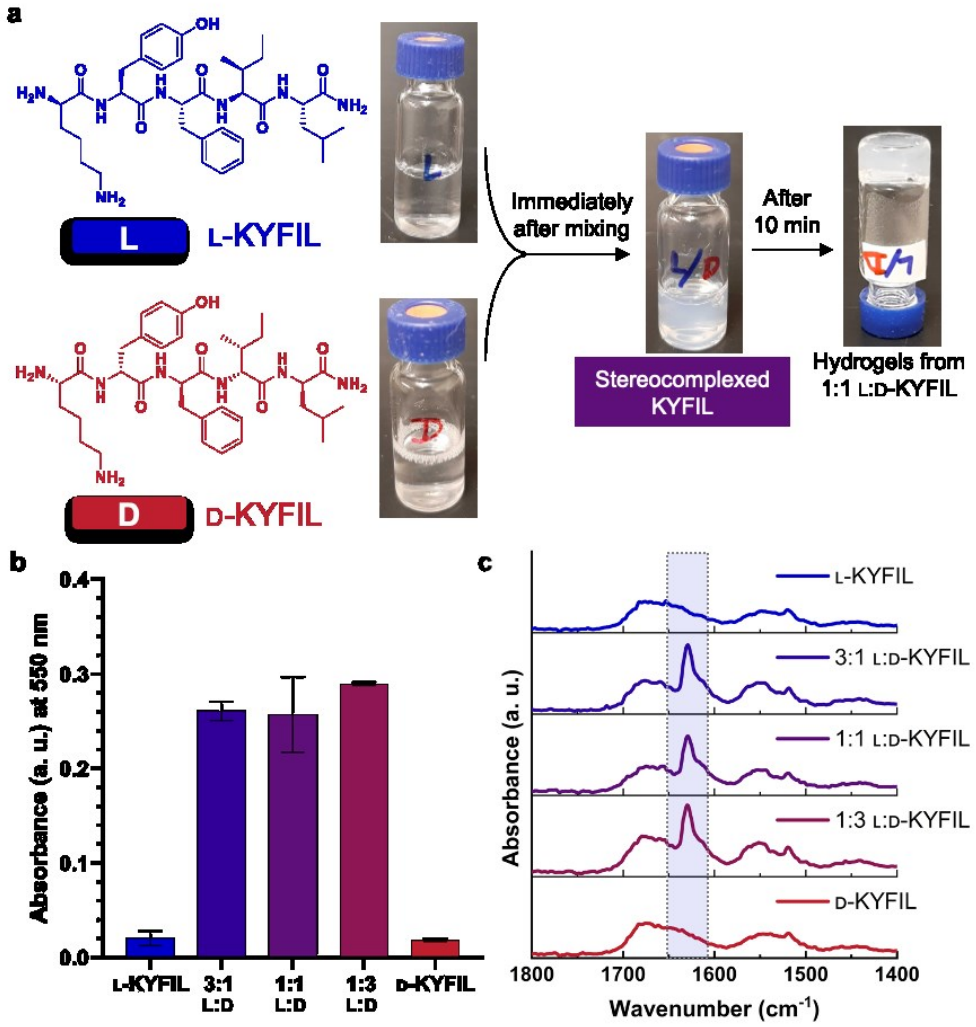

Figure 1. Stereocomplexation of L- and D-KYFIL at 3% (w/v) in water: (a) individually, L- and D-peptides remain soluble, while their 1:1 mixtures form turbid solutions, then gel; (b) turbidity of L- and D-KYFIL solutions and their blends (L:D = 3:1, 1:1, and 1:3), gauged by absorbance at 550 nm; (c) FTIR spectra of L- and D-KYFIL and their blends (L:D = 3:1, 1:1, and 1:3). Spectra of the blends feature an amide I carbonyl stretch absorption around 1630 cm^{-1}, characteristic of β-sheets, whereas this peak is absent in the spectra of solutions containing only L- or D-KYFIL.

Evidence of KYFIL peptide stereocomplexation in water. While L-KYFIL peptides form fibrous hydrogels at 3% (w/v) in 1X PBS at pH 7.4[41], both L- and D-KYFIL are soluble at the same concentration in pure water (Figure 1a), likely due to the protonation of amines (i.e., on lysine (K) and the N-terminus) and/or to electrostatic repulsion between them. Blending L- and D-KYFIL solutions at 3% (w/v) in water at 3:1, 1:1 and 1:3 volumetric ratio yields turbid solutions immediately that gel within

10 min (Videos 1-4). Turbidity measurements taken after mixing show ~10 times higher absorbance from all of the blends than from the solutions of L- and D-KYFIL alone (Figure 1b). Consistent with the turbidity measurements, transmission electron microscopy (TEM) of the 1:1 L:D KYFIL blend shows large, albeit relatively ill-defined structures, whereas images of the constituents show no appreciable structure formation (Figures S17-S26).

We next acquired Fourier transformed infrared (FTIR) spectra to gain insight about peptide structure at the molecular level, namely the presence or absence of β-sheet secondary structure characteristic of fibrous L-KYFIL hydrogels. At 3 % (w/v) in water, FT-IR spectra of L- and D-KYFIL do not contain the characteristic β-sheet absorbances at 1627-1635 cm^{-1} corresponding to amide I carbonyl stretching (boxed in Figure 1c). Spectra of the 3:1, 1:1, and 1:3 L:D-KYFIL blends, however, prominently feature these characteristic absorbances. The presence of β-sheets in all of the blends, contrasted with the absence of defined secondary structure in the L- and D-constituents, highlights the impact of stereocomplexation on peptide secondary structure.

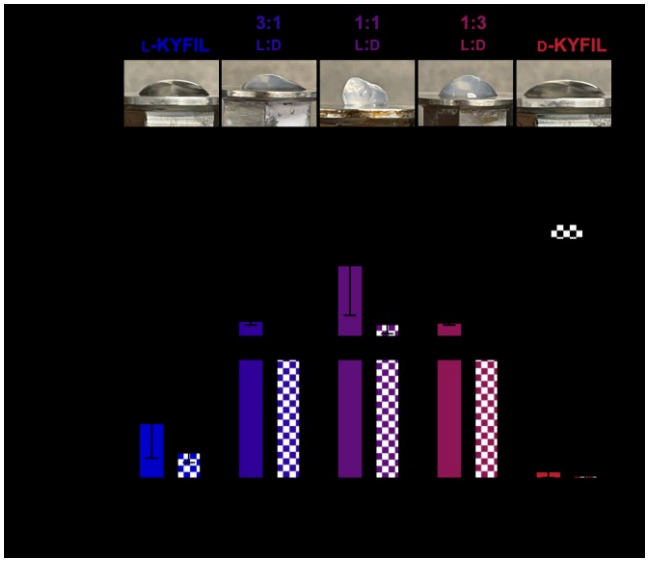

Figure 2. Rheology of KYFIL as a function of stereochemical composition at 3% (w/v) in water. (a) Images of liquid L- and D-KYFIL peptide solutions and elastic 1:1 L:D-KYFIL hydrogels 30 min after preparation in water; and (b) shear moduli of L- and D-KYFIL solutions and gels formed from their 1:1 blends. Storage (G') and loss (G'') moduli are reported as the average modulus measured between 1-10 rad/s from 3 independently prepared samples, with error bars representing standard deviation.

At the macroscopic scale, L- and D-KYFIL individually dissolve in water at 3% (w/v) while their blends form self-supporting gels (Figure 2). Photographs and rheology data attest to the elastic, gel-like behavior of 1:1 L:D-KYFIL blends (G' = 2.4 ± 1.7 kPa, G" = 0.4 ± 0.3 kPa) and the liquid-like behavior of L-KYFIL (shear storage modulus G' = 0.005 ± 0.002 kPa, loss modulus G" = 0.002 ± 0.001 kPa) and D-KYFIL (G' = 0.0006 ± 0.0005 kPa, G" = 0.0003 ± 0.0003 kPa). While G' approximately equals G" for L-KYFIL and D-KYFIL individually in water, the photographs in Figure 2a and Videos 1-2 showcase the liquid-like natures of these solutions. We suspect that the parallel plate geometry selected to accommodate the hydrogel samples led to low signal to noise ratio and higher variability in these liquid samples. The intermediate 1:3 and 3:1 L:D-KYFIL blends show moduli intermediate between the individual constituents and the 1:1 blends, which is particularly apparent in the full frequency and strain sweeps provided in Figures S6-S8. The marked changes in rheological properties, solubility, and secondary structure we observe upon blending L- and D-KYFIL in water, even in unequal ratios, provide convincing evidence of stereocomplexation.

Stereocomplexation of KYFIL in PBS. We next investigated how physiological conditions, namely 1X PBS adjusted to pH 7.4, impact KYFIL stereochemistry-directed assembly on the molecular and bulk scale. This presented more of a challenge because unlike in water, where we observe an obvious transition from dissolved peptide solutions to gels upon stereocomplexation, the assembly and gelation of the individual constituents under physiological conditions makes stereocomplexation less visually apparent. Indeed, as reported previously, L-KYFIL forms hydrogels at 3% (w/v) in PBS at pH 7.4, and D-KYFIL does the same. Blends of L- and D-KYFIL, including L:D ratios = 3:1, 1:1, and 1:3 also yield self-supporting hydrogels (Figure 3a). Consistent with the molecular assembly we observe regardless of stereochemical composition, FTIR spectroscopy provides evidence of β-sheets in all formulations (Figure S4). While these qualitative visual observations and spectroscopic data show similarities across all formulations, we expected that stereocomplexation may be occurring and so we moved to quantify the rheological properties of these materials.

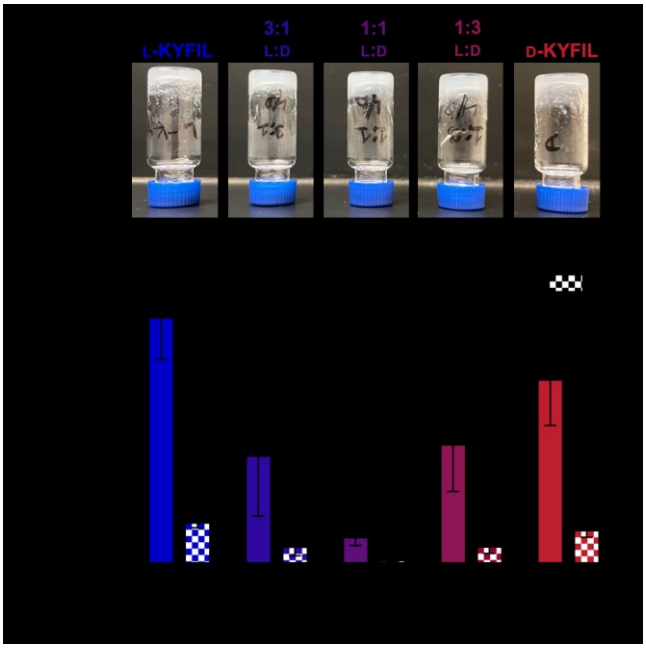

Figure 3. Rheology of KYFIL hydrogels (method 2) as a function of stereochemical composition at 3% (w/v) in 1X PBS at pH 7.4. (a) Images showing that L-, 3:1 L:D-, 1:1 L:D-, 1:3 L:D- and D-KYFIL formulations all form gels 30 min after preparation; (b) shear moduli of hydrogels from L- and D-KYFIL and their blends in PBS showing that stiffness decreases as the L:D ratio approaches 1:1. Shear moduli are reported as the averages over 1-10 rad/s from 3 independently prepared samples, with error bars representing standard deviation.

Given the evidence of stereochemistry-promoted hydrogelation of KYFIL peptides in water and the literature precedent for enantiomeric peptide mixtures to enhance mechanics, we expected blends of L- and D-KYFIL would produce stiffer hydrogels. Hydrogels from individual L- and D-KYFIL maintain

elastic behavior throughout the 0.01-1% strain and 0.1-100 rad/s frequency range (Figure S9-S12). The average moduli of D-KYFIL at 3% (w/v) (G' = 23 ± 6 kPa, G" = 4 ± 0.8 kPa) are similar to those of L-KYFIL (G' = 31 ± 5 kPa , G" = 5 ± 0.6 kPa) (Figure 3b). Surprisingly, the 1:1 L:D-KYFIL hydrogels have significantly lower moduli (G' = 3 ± 1 kPa, G" = 0.4 ± 0.1 kPa) than L-and D-hydrogels. Intermediate ratios of 3:1 L:D-KYFIL (G' = 14 ± 8 kPa, G'' = 5 ± 0.6 kPa) and 1:3 L:D-KYFIL (G' = 15 ± 6 kPa, G'' = 2 ± 0.8 kPa form less stiff hydrogels than pure enantiomers, but stiffer than 1:1 L:D-KYFIL blends. While the absolute values of the moduli depend on the hydrogel preparation method, concentration, pH and the rheometer gap height (Figures S13-S16), under all test conditions, stiffness decreases as the ratio of L-KYFIL:D-KYFIL approaches 1:1. Interestingly, at lower peptide concentrations, i.e. 1.5% (w/v), although individual L- and D-KYFIL still form hydrogels, the 1:1 L:D-KYFIL blends form colloidal suspensions that do not pass the inversion test (Figure S5). Suspecting differences in morphology may be responsible for the observed mechanics, we investigated how stereochemistry impacts KYFIL biomaterials at the nanoscale.

Effect of stereocomplexation on morphology. To examine how KYFIL stereocomplexation impacts morphology, we imaged L- and D-KYFIL and their blends in PBS at pH 7.4 using TEM. Since the 3% (w/v) concentration used in other experiments generated films on TEM grids that were too dense to image effectively, we also acquired images at 0.75 and 1.5% (w/v). Consistent with previous reports of L-KYFIL morphology in 1X PBS at pH 7.4,[41] L-KYFIL yields twisted nanoscale fibers with an average diameter of 22 ± 3.5 nm and an average pitch 104 ± 11 nm (Figures 4, S27, S32, S37 and S42). These dimensions are similar to D-KYFIL fibers that have an average diameter of 26 ± 4 nm and twist with an average pitch of 122 ± 17 nm (Figures 4, S31, S36, S41 and S42). Blending L- and D-KYFIL produced a striking morphological transformation; instead of nanoscale fibers, the 1:1 blend forms micron-scale sheets ranging in width from 100 to 550 nm (Figures 4, S29, S34, S39, S43). Intermediate 3:1 L:D and 1:3 L:D ratio samples form a mixture of twisted fibers and flat sheets, suggesting that excess L-KYFIL or D-KYFIL in enantiomeric blends forms fibers (Figures 4, S28, S30, S33, S35, S38, S40, S42-43). While image quality improved as we decreased concentration from 3% (w/v) to 0.75% (w/v), the morphologies remain consistent as a function of L:D-KYFIL ratio (Figures S24-S38).

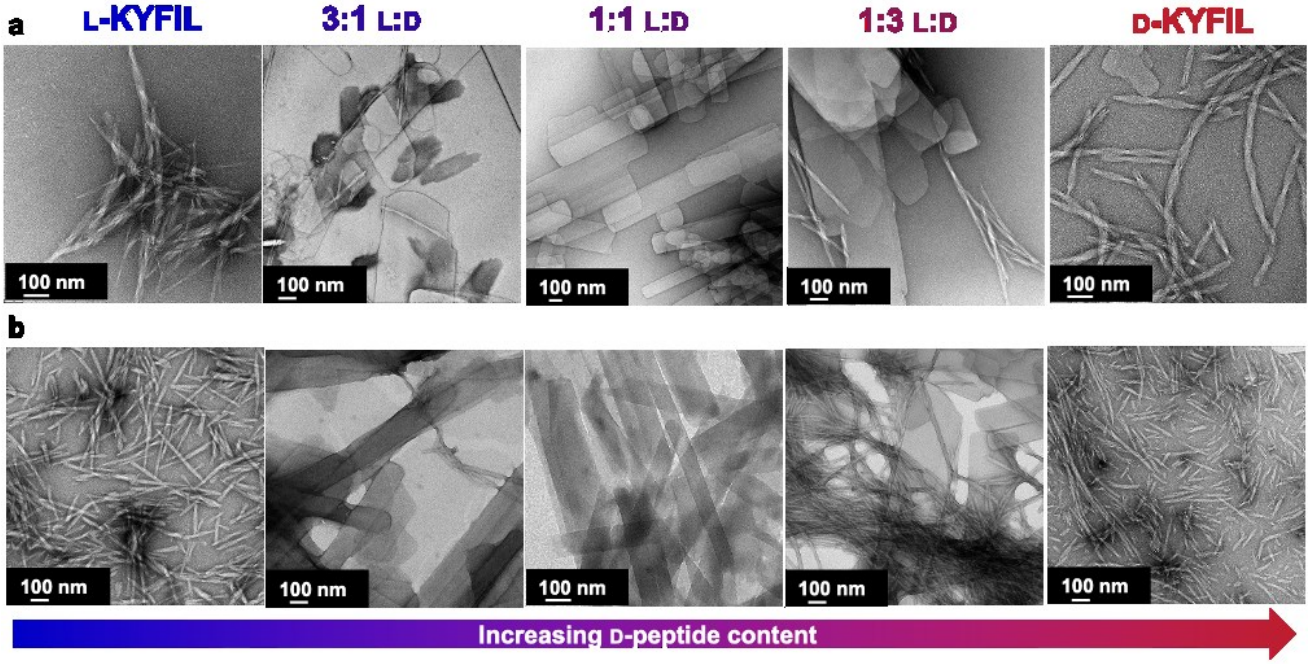

Figure 4. Stereochemistry-directed morphology changes in KYFIL hydrogels (method 1, 1X PBS at pH 7.4). TEM images of L-, 3:1 L:D-, 1:1 L:D-, 1:3 L:D- and D-KYFIL samples at (a) 0.75% (w/v) and (b) 1.5% (w/v), respectively. Only nanoscale fibers are found in pure D- and L-KYFIL samples, while 1:1 L:D-KYFIL blends form exclusively plates. The intermediate 3:1 L:D and 1:3 L:D-KYFIL samples contain a mixture of plates and fibers.

The morphological transition from entangleable fibers to micron-scale plates upon blending L- and D-KYFIL explains the lower stiffness of the stereocomplexed hydrogels in presence of salt. In hydrogels containing only L-KYFIL or only D-KYFIL, entanglement and interaction of the twisted, peptide fibers create a gelled 3D network. However, the plates formed upon blending the enantiomers are unlikely to entangle, and instead simply disperse in solution and scatter light to form milky, liquid-like solutions or at high concentrations, weak networks. The presence of entangleable fibers in addition to plates in the intermediate 3:1 L:D- and 1:3 L:D-KYFIL blends is consistent with these samples exhibiting mechanics intermediate between those of the 1:1 blend containing only plates and the fibrous hydrogels formed from the L-KYFIL and D-KYFIL constituents. By independently forming hydrogels from L-KYFIL and D-KYFIL in PBS, then blending the two fibrous formulations, we created mixtures of fibers and plates observed both 30 min and 1 week after mixing. Using this particular mixing strategy, we also witness previously unobserved structures that appear to be aligned fibers or plates at both the 30 min and 1 week time

points (Figures S52-S53). Rheology showed samples after 1 week had a slight reduction of modulus compared to the 30 min timepoint (Figures S54-S55). The dynamic evolution of morphology and accompanying materials properties of peptides upon stereocomplexation raises intriguing questions for future pursuit.

At first glance, the lower stiffness of the 1:1 blends of L- and D-KYFIL seem to contrast prior reports showing blends of L- and D-peptides to yield stiffer hydrogels. However, in these previous reports, the blends retain the nanoscale fibrous morphology conducive to entanglement and gelation[35–38]. The enhanced stiffness in these cases is attributed to the formation of more rigid fibers upon blending L- and D-peptides, a conclusion arrived at after diffusing wave spectroscopy revealed blends of L- and D-MAX1 peptides to form more rigid fibers than those from either constituent[35–37]. In contrast, Nilsson and coworkers observed a remarkably similar morphology change as we did, from nanoscale fibers to micron-scale plates, upon blending L- and D-forms of the amyloid-β peptide Ac-(KLVFFAE)$_2$-NH$_2$[37,40]. Mechanics and gelation were not the focus of their study and were therefore not reported, but based on our results, we would expect the stiffnesses of the blended amyloid-β (16-22) peptide hydrogels to be lower than those from pure L- or D-peptide hydrogels.

Considered together, these findings showcase that the morphologies and mechanics that result from blending L- and D-peptides are sequence-specific. Both KYFIL and Ac-(KLVFFAE)$_2$-NH$_2$ peptides, which transition from fibrous hydrogels to dispersions of plates upon stereocomplexation, contain stretches of 4 hydrophobic amino acids, whereas the MAX1 and Ac-(FKFE)$_2$-NH$_2$ peptides that retain the fibrous hydrogel morphology feature alternating hydrophilic and hydrophobic residues. The arrangement of hydrophobic residues in the peptide sequence offers a possible explanation for how morphology, and by extension mechanics, change with peptide sequence, and is something we plan to probe in future work using a longer peptide with a more regular sequence pattern such as Ac-(FKFE)$_2$. Given that, in addition to changes in mechanics and morphology, material lifetime changes are a prominent feature of stereocomplexed materials, we next moved to determine how blending L- and D-KYFIL impacted proteolytic stability.

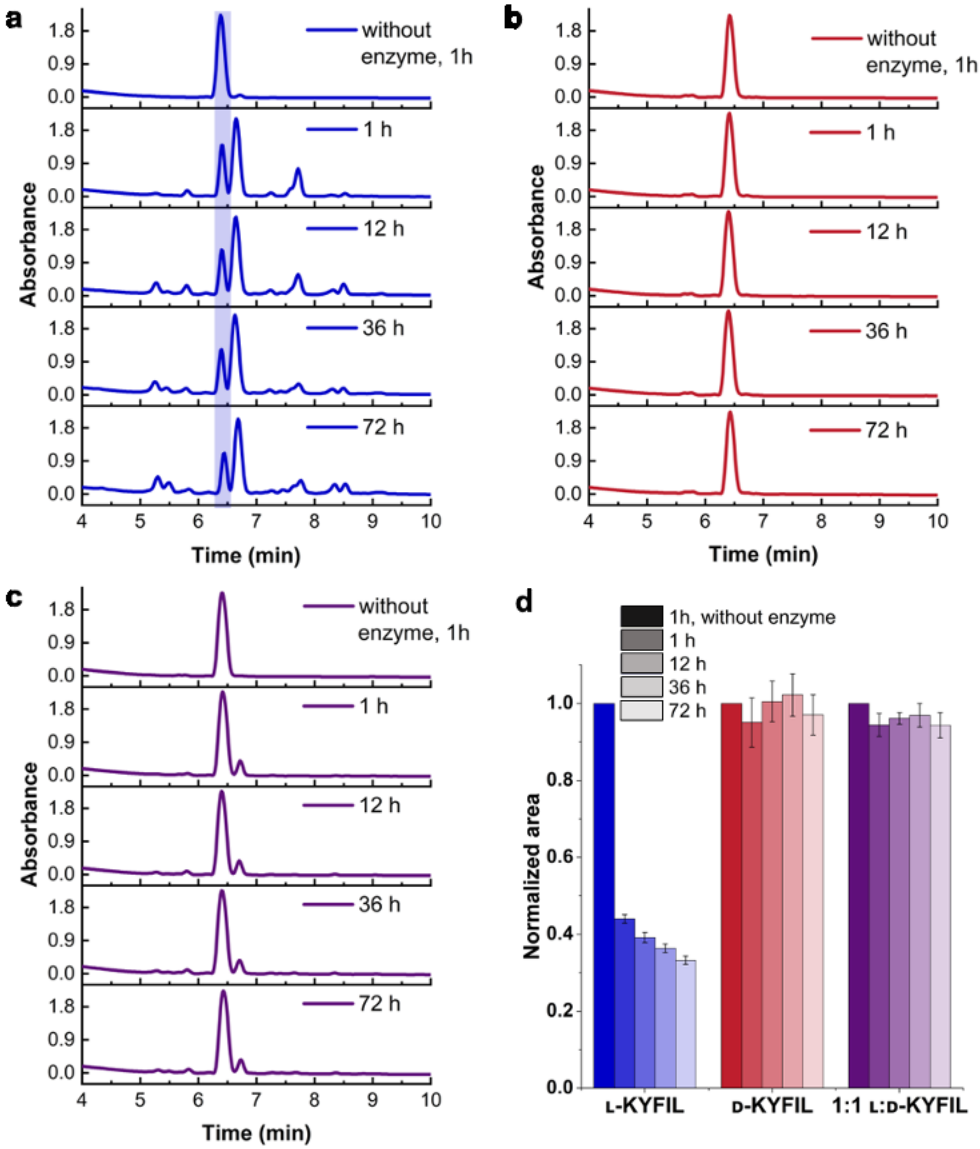

Figure 5. Proteolytic stability of KYFIL hydrogels (method 1) at 3% (w/v) in the presence of 0.2 mg/mL Proteinase K. HPLC chromatograms of (a) L-KYFIL hydrogels, (b) D-KYFIL hydrogels and (c) 1:1 L:D-KYFIL hydrogels after 1, 12, 36, and 72 h. The appearance of new peaks following incubation with protease indicates degradation of L-KYFIL, whereas we observe no degradation is observed of D-KYFIL and little evidence of degradation in the 1:1 L:D-KYFIL hydrogels. (d) Percent intact KYFIL after 1, 12, 36, and 72 h incubation with Proteinase K, showing 1:1 L:D-KYFIL hydrogels to remain largely stable, with >90% KYFIL remaining intact after 72 h. The error bars represent standard deviation, with n = 3 samples.

Effect of peptide stereocomplexation on proteolytic stability. While naturally abundant L-peptides are susceptible to proteolytic degradation, D-peptides are known to be resistant. Blending L-peptides with D-peptides is known to improve the proteolytic stability of the L-component[39]. Given that stereocomplexation transformed the morphology and mechanics of KYFIL biomaterials, we were interested in how these interactions would impact proteolytic stability. To this end, we incubated L-, 1:1 L:D-, D-KYFIL hydrogels with Proteinase K, a broadly active protease predicted to cleave L-KYFIL between the Y-F, F-I, and I-L residues[43]. After 1, 12, 36, and 72 h incubations, we added dimethyl sulfoxide (DMSO) to solubilize the peptides and deactivate Proteinase K prior to analysis. We used high-performance liquid chromatography (HPLC) to determine the percentage of peptide remaining intact as a function of incubation time. In the absence of Proteinase K, both L- and D-KYFIL, individually and blended, elute at 6.4 min as a single peak, exhibiting no appreciable degradation over the 72 h duration of the experiment (Figure 5 and Figures S44-S46). However, after just 1 h of incubation with Proteinase K, only ~40% L-KYFIL remains intact and new peaks appear in the chromatograms at ~6.8 and ~7.8 min, likely associated with L-KYFIL degradation products (Figure 5a). Continued incubation of L-KYFIL samples for up to 72 h results in additional peaks between 5-6 min and 7-8 min, indicating further degradation. Yet, the proteolysis slows after the first hour, with ~35% L-KYFIL remaining after 72 h (Figure 5d). Consistent with the expected proteolytic stability of D-peptides, protease-treated D-KYFIL samples remained intact for the entire duration of the experiment (Figure 5b). The 1:1 L:D-KYFIL blend incubated with protease degraded less than 10% over the 72 h experiment, with just one small new peak appearing in the chromatograms at ~6.8 min (Figure 5c and Figure S45). If stereochemistry-directed assembly did not protect the L-peptides from degradation, we would expect 50% reduction in the peak corresponding to intact KYFIL.

While differences in KYFIL stereocomplex morphology (plates) relative to the individual L- and D-peptides (nanofibers) may contribute to the observed differences in proteolytic stability, our results are remarkably similar to those on L- and D-Ac-$(FKFE)_2$-NH_2. In this previously documented system, stereocomplexation confers proteolytic stability to the L-peptide, however the stereocomplexed mixture retains the nanoscale fibrous morphology of the individual peptides. Together with prior reports, our results highlight the role of stereochemistry-directed interactions in tempering proteolytic degradation, therein offering a strategy to control biomaterial lifetime.

Blending complementary stereoisomers orchestrates molecular packing. We have seen thus far that blending L- and D-peptides transforms biomaterial morphology, mechanics, and stability, and sought to determine whether these changes resulted from differences in molecular packing. We performed X-ray diffraction on L- and D-KYFIL and their 1:1 L:D blends by dispersing or dissolving the peptide at 3% (w/v) in water or 1X PBS peptide, followed by lyophilization. All patterns for samples prepared in PBS contain intense peaks between 2θ = 25° to 65° (Figure S49). Neither L-KYFIL nor D-KYFIL samples showed evidence of crystallinity, as gleaned by the absence of peaks in the XRD patterns other than those attributable to PBS salts (Figure 6). In contrast, the patterns of 1:1 L:D-KYFIL blends prepared in both water and PBS pattern feature prominent diffraction peaks at 8.6° and 19.4°, as well as three less intense peaks at 17°, 21° and 25° (Figure 6 and Figure S50). The distinct features of 1:1 L:D-KYFIL patterns relative to those of the constituent peptides indicates that blending L- and D-KYFIL indeed directs packing of peptides at the molecular level, consistent with the changes we observe in bulk properties. These findings of specific interactions between complementary stereoregular peptides directing molecular packing and transforming material properties are entirely akin to stereocomplexation of synthetic polymers. Thus, we term these assemblies of L- and D-KYFIL 'peptide stereocomplexes' in an effort to bring together knowledge from both the peptide and synthetic polymer fields to inform molecular design rules governing stereochemistry-directed assembly for advanced materials as designer biomaterials and for application in other sectors.

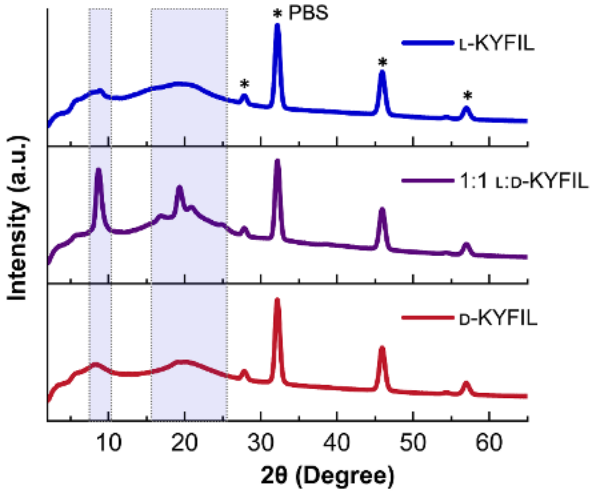

Figure 6. X-ray diffraction patterns of L-, 1:1 L:D-, D-KYFIL in PBS. L- and D-KYFIL patterns lack sharp peaks that are not attributed to PBS, while the pattern of their 1:1 blend shows prominent diffraction peaks between 2θ = 2° and 25° (highlighted), indicating a change in molecular packing. The diffraction peaks in all three patterns between 2θ = 25° and 65° (denoted with *) arise from the crystalline salts in PBS.

CONCLUSIONS

Together, this work highlights how stereocomplexation orchestrates peptide supramolecular assembly and modulates biomaterial mechanical properties, morphology, and proteolytic stability. First, experiments in water provided spectroscopic, visual, and rheological evidence of the specific interactions between the L- and D-isomers of the RAPID peptide KYFIL. In solutions with physiological salt and pH, where L- and D-KYFIL self-assemble into entangled fibrous hydrogels, blending the two isomers produced a striking decrease in hydrogel

stiffness explained by the morphological transformation into unentangleable micron-scale plates. This finding contrasts prior reports of enhanced stiffness and retention of fibrous morphology upon blending L- and D-peptides. In all cases, the morphological changes that occur upon stereocomplexation offer an explanation for the resulting mechanical properties. Yet the different outcomes with different peptide systems raise exciting new questions about the role of peptide sequence in stereochemistry-directed assembly. Moreover, stereocomplexation of KYFIL confers proteolytic stability, providing opportunities to control material lifetime. Additionally, the 1:1 blends have comparable proteolytic stability to D-KYFIL, but a distinctive 2D plate morphology that may confer unique therapeutic release and cell behavior in biomaterials.

Akin to stereocomplexation of synthetic polymers, x-ray diffraction revealed changes in molecular packing upon KYFIL stereocomplexation to underpin the changes we observe in morphology, mechanics, and stability. Knowledge from the synthetic polymer stereocomplexation literature has and will continue to inform design of peptide-based stereocomplexes, and in turn, we expect that learning the design rules of peptide stereocomplexation will contribute to the development of stereocomplexed polymers. Going forward, continuing to correlate peptide sequence to the molecular-level and bulk properties of stereocomplexed biomaterials will provide critical insights into this emerging molecular design tool to tailor biomaterial properties to mimic native tissue.

EXPERIMENTAL METHODS

Hydrogel formation

In water (for rheology). We prepared 3% (w/v) solutions of L- and D-KYFIL by dissolution of peptide in ultrapure water with stirring. For L:D-KYFIL blends, we mixed the L-and D-peptide solutions in three different volumetric ratios: 3:1, 1:1 and 1:3. The mixtures formed self-supporting hydrogels within 10 min.

In PBS (pH 7.4). Over the course of this study, we employed two methods to prepare hydrogels in PBS at pH 7.4; these are illustrated schematically in Figures S1-S2. Briefly, Method 1 involves first dissolving L-KYFIL and D-KYFIL in water prior to blending if relevant (i.e., for blends of 3:1, 1:1, and 1:3 L-KYFIL: D-KYFIL) and then adding PBS and adjusting pH to induce assembly and gel formation. Method 2, used in our previous reports on L-KYFIL[41], involves dispersion of L- and D-peptide powders and their blends directly into solutions that promote gelation (i.e., PBS for L- and D-KYFIL and water for their blends), followed by addition of PBS (in the case of the blends) and pH adjustment. While Methods 1 and 2 yield hydrogels with different stiffnesses, the trends in stiffness as a function of stereochemical composition remain the same regardless of preparation method (Figure S10).

Circular dichroism (CD) spectroscopy. To confirm peptide stereochemistry, we recorded circular dichroism (CD) spectra of L-, 3:1 L:D-, 1:1 L:D-, 1:3 L:D- and D-KYFIL at 0.2% (w/v) in water on a Jasco J-1500 CD spectrophotometer with a 0.1 mm path length quartz cuvette from 250 nm to 190 nm at a continuous scan speed of 50 nm/min at 25°C. Three scans were obtained for each solution, and each scan was corrected with a background ultrapure water scan.

Absorbance measurements. To gauge changes in peptide solubility in pure water resulting from stereocomplexation, absorbance measurements were obtained with L- and D-KYFIL solutions and their blends (3:1, 1:1 and 1:3) at 3% (w/v) in ultrapure water using 96-well plates at 550 nm with a Biotek Synergy 4 plate reader.

Fourier transformed infrared (FTIR) spectroscopy. For determination of peptide secondary structure, we acquired Fourier transform infrared (FTIR) spectra of 3.0% (w/v) formulations of L-, 3:1 L:D-, 1:1 L:D-, 1:3 L:D- and D-KYFIL peptides in water and 1X PBS (pH 7.4). The spectra were collected on a PerkinElmer 400 FT-IR spectrometer equipped with an attenuated total reflectance (ATR) accessory at 1 cm^{-1} resolution, and subtracted the background spectra (water or 1X PBS).

Rheology. Oscillatory shear rheology was performed on samples prepared in water (Figure 2) and in 1X PBS at pH 7.4 by method 2 (Figure 3) 30 min after preparation. Water and PBS samples were measured at 25 °C on an Anton Paar MCR 302e rheometer (25 mm parallel plate) and a TA Instruments DHR-3 rheometer (20 mm solvent-trap parallel plate) respectively. Amplitude sweeps (0.01-100%) were conducted at a constant angular frequency of 10 rad/s and a gap height of 100 μm. Frequency sweeps (0.1-100 rad/s) were performed at a constant strain of 1% within the linear viscoelastic range.

Transmission Electron Microscopy (TEM). TEM images were acquired for L-, 3:1 L:D-, 1:1 L:D-, 1:3 L:D- and D-KYFIL in water at 0.75% (w/v) and 3% (w/v) and in PBS (pH 7.4) at 0.75% (w/v), 1.5% (w/v) and 3% (w/v) (method 1). Samples imaged on carbon grids after staining with 2% (w/v) uranyl acetate in an F20 electron microscope (Thermo-Fisher) operating at 120 kV at magnifications ranging from 3200X-62000X and recorded on a TVIPS XF416 camera (Teitz).

Proteolytic stability measurements. To assess the impact of stereocomplexation on proteolytic stability, we incubated the L-, 1:1 L:D-, and D-KYFIL hydrogels in Proteinase K and monitored the concentration of intact peptide as a function of incubation time (1 h, 12 h, 36 h and 72 h). Hydrogels were prepared similarly in the absence of enzyme for control experiments. Following incubation of the hydrogels for the desired time, DMSO was added to dissolve the gels and deactivate Proteinase K, and then HPLC was performed on a Waters Alliance e2695 XC HPLC system to measure the percentage of intact peptide by the comparison of the peak corresponding to intact peptide relative to the total integration of peptide peaks. Elution of peptide and degradation products were monitored at 214 nm.

X-ray diffraction (XRD) experiments. Powder x-ray diffraction patterns were recorded for L-KYFIL, D-KYFIL, and their 1:1 blends. The samples were mounted on a MiTeGen MicroLoop holder and then diffraction patterns were acquired using Bruker D8 Venture Photon III Kappa four-circle diffractometer system. The patterns were analyzed with APEX4 Software.

ASSOCIATED CONTENT

Supporting Information

The Supporting Information is available free of charge on the ACS Publications website.

Materials, additional experimental details, additional figures and associated discussions for CD spectroscopy, FT-IR spectroscopy, rheological characterization, TEM images, HPLC traces for proteolytic stability measurement and X-ray diffraction patterns (PDF)

Video 1. L-KYFIL peptide in water (MP4)
Video 2. D-KYFIL peptide in water (MP4)

Video 3. Mixing L- and D-KYFIL in water at 1:1 L:D volumetric ratio (MP4)
Video 4. Hydrogel formation of 1:1 L:D-KYFIL in water after 10 min of preparation (MP4)

AUTHOR INFORMATION

Corresponding Authors

Kyle J. Lampe - Department of Chemical Engineering, University of Virginia, Charlottesville VA 22903, Email: lampe@virginia.edu
Rachel A. Letteri - Department of Chemical Engineering, University of Virginia, Charlottesville VA 22903, Email: rl2qm@virginia.edu

Present Addresses

Connor D. Amelung, Department of Biomedical Engineering, Duke University, Durham, NC, 27705.

Author Contributions

I. D., J. F. C.A., V.G., R. L., and K. L. conceived the idea and designed experiments. I. D., J. F., and V. G., conducted experiments and associated analysis. A. K. analyzed TEM images. I. D., J. F., K. L., and R. L. wrote the manuscript with input from all authors. R. L. and K. L. supervised the work.

Funding Sources

The authors gratefully acknowledge financial support from the National Science Foundation (BMAT-2143647 – R.A.L.; BMAT-2104723 – K.J.L.) and the Commonwealth Health Research Board of Virginia (K.J.L.). V. P. G. acknowledges financial support from a National Institutes of Health Biotechnology Training Program (T32GM136615).

ACKNOWLEDGMENT

For acquiring some of the TEM images, the authors acknowledge Kelly Dryden (Associate Professor of Research, Molecular Physiology and Biological Physics) at the University of Virginia Molecular Electron Microscopy Core facility (RRID:SCR_019031), which is supported in part by the School of Medicine and was built with NIH grant G20-RR31199. For assistance with acquiring x-ray diffraction patterns, the authors acknowledge Diane Dickie and the University of Virginia X-ray diffraction lab funded by the NSF-MRI program (CHE-2018870).

ABBREVIATIONS

RAPID, rapidly assembling pentapeptides for injectable delivery; G', storage modulus; G", loss modulus; FTIR, Fourier transformed infrared spectroscopy; CD, Circular dichroism; HPLC, high-performance liquid chromatography; TEM, transmission election microscopy; XRD, X-ray diffraction.

REFERENCES

(1) Kirillova, A.; Yeazel, T. R.; Asheghali, D.; Petersen, S. R.; Dort, S.; Gall, K.; Becker, M. L. Fabrication of Biomedical Scaffolds Using Biodegradable Polymers. *Chem. Rev.* **2021**, *121* (18), 11238–11304. https://doi.org/10.1021/acs.chemrev.0c01200.

(2) Peterson, G. I.; Dobrynin, A. V.; Becker, M. L. Biodegradable Shape Memory Polymers in Medicine. *Adv. Healthc. Mater.* **2017**, *6* (21), 1700694. https://doi.org/10.1002/adhm.201700694.

(3) Webber, M. J.; Khan, O. F.; Sydlik, S. A.; Tang, B. C.; Langer, R. A Perspective on the Clinical Translation of Scaffolds for Tissue Engineering. *Ann. Biomed. Eng.* **2015**, *43* (3), 641–656. https://doi.org/10.1007/s10439-014-1104-7.

(4) Webber, M. J.; Appel, E. A.; Meijer, E. W.; Langer, R. Supramolecular Biomaterials. *Nat. Mater.* **2016**, *15* (1), 13–26. https://doi.org/10.1038/nmat4474.

(5) Straley, K. S.; Foo, C. W. P.; Heilshorn, S. C. Biomaterial Design Strategies for the Treatment of Spinal Cord Injuries. *J. Neurotrauma* **2010**, *27* (1), 1–19. https://doi.org/10.1089/neu.2009.0948.

(6) Barreto-Ortiz, S. F.; Zhang, S.; Davenport, M.; Fradkin, J.; Ginn, B.; Mao, H.-Q.; Gerecht, S. A Novel In Vitro Model for Microvasculature Reveals Regulation of Circumferential ECM Organization by Curvature. *PLoS ONE* **2013**, *8* (11), e81061. https://doi.org/10.1371/journal.pone.0081061.

(7) Caliari, S. R.; Burdick, J. A. A Practical Guide to Hydrogels for Cell Culture. *Nat. Methods* **2016**, *13* (5), 405–414. https://doi.org/10.1038/nmeth.3839.

(8) Tibbitt, M. W.; Anseth, K. S. Hydrogels as Extracellular Matrix Mimics for 3D Cell Culture. *Biotechnol. Bioeng.* **2009**, *103* (4), 655–663. https://doi.org/10.1002/bit.22361.

(9) Ulrich, T. A.; de Juan Pardo, E. M.; Kumar, S. The Mechanical Rigidity of the Extracellular Matrix Regulates the Structure, Motility, and Proliferation of Glioma Cells. *Cancer Res.* **2009**, *69* (10), 4167–4174. https://doi.org/10.1158/0008-5472.CAN-08-4859.

(10) Hilderbrand, A. M.; Ford, E. M.; Guo, C.; Sloppy, J. D.; Kloxin, A. M. Hierarchically Structured Hydrogels Utilizing Multifunctional Assembling Peptides for 3D Cell Culture. *Biomater. Sci.* **2020**, *8* (5), 1256–1269. https://doi.org/10.1039/C9BM01894H.

(11) Godbe, J. M.; Freeman, R.; Burbulla, L. F.; Lewis, J.; Krainc, D.; Stupp, S. I. Gelator Length Precisely Tunes Supramolecular Hydrogel Stiffness and Neuronal Phenotype in 3D Culture. *ACS Biomater. Sci. Eng.* **2020**, *6* (2), 1196–1207. https://doi.org/10.1021/acsbiomaterials.9b01585.

(12) Lewis, D. M.; Blatchley, M. R.; Park, K. M.; Gerecht, S. O2-Controllable Hydrogels for Studying Cellular Responses to Hypoxic Gradients in Three Dimensions in Vitro and in Vivo. *Nat. Protoc.* **2017**, *12* (8), 1620–1638. https://doi.org/10.1038/nprot.2017.059.

(13) Rodell, C. B.; MacArthur, J. W.; Dorsey, S. M.; Wade, R. J.; Wang, L. L.; Woo, Y. J.; Burdick, J. A. Shear-Thinning Supramolecular Hydrogels with Secondary Autonomous Covalent Crosslinking to Modulate Viscoelastic Properties In Vivo. *Adv. Funct. Mater.* **2015**, *25* (4), 636–644. https://doi.org/10.1002/adfm.201403550.

(14) Yamada, Y.; Patel, N. L.; Kalen, J. D.; Schneider, J. P. Design of a Peptide-Based Electronegative Hydrogel for the Direct Encapsulation, 3D Culturing, in Vivo Syringe-Based Delivery, and Long-Term Tissue Engraftment of Cells. *ACS Appl. Mater. Interfaces* **2019**, *11* (38), 34688–34697. https://doi.org/10.1021/acsami.9b12152.

(15) Dobbs, R.; Choe, S.; Kalmanek, E.; Harrington, D. A.; Stupp, S. I.; McVary, K. T.; Podlasek, C. A. Peptide Amphiphile Delivery of Sonic Hedgehog Protein Promotes Neurite Formation in Penile Projecting Neurons. *Nanomedicine Nanotechnol. Biol. Med.* **2018**, *14* (7), 2087–2094. https://doi.org/10.1016/j.nano.2018.06.006.

(16) Collier, J. H.; Rudra, J. S.; Gasiorowski, J. Z.; Jung, J. P. Multi-Component Extracellular Matrices Based on Peptide Self-Assembly. *Chem. Soc. Rev.* **2010**, *39* (9), 3413. https://doi.org/10.1039/b914337h.

(17) Collier, J. H.; Segura, T. Evolving the Use of Peptides as Components of Biomaterials. *Biomaterials* **2011**, *32* (18), 4198–4204. https://doi.org/10.1016/j.biomaterials.2011.02.030.

(18) O'Leary, L. E. R.; Fallas, J. A.; Bakota, E. L.; Kang, M. K.; Hartgerink, J. D. Multi-Hierarchical Self-Assembly of a Collagen Mimetic Peptide from Triple Helix to Nanofibre and Hydrogel. *Nat. Chem.* **2011**, *3* (10), 821–828. https://doi.org/10.1038/nchem.1123.

(19) Cui, H.; Webber, M. J.; Stupp, S. I. Self-Assembly of Peptide Amphiphiles: From Molecules to Nanostructures to Biomaterials. *Biopolymers* **2010**, *94* (1), 1–18. https://doi.org/10.1002/bip.21328.

(20) Hartgerink, J. D.; Beniash, E.; Stupp, S. I. Peptide-Amphiphile Nanofibers: A Versatile Scaffold for the Preparation of Self-Assembling Materials. *Proc. Natl. Acad. Sci.* **2002**, *99* (8), 5133–5138. https://doi.org/10.1073/pnas.072699999.

(21) Gray, V. P.; Amelung, C. D.; Duti, I. J.; Laudermilch, E. G.; Letteri, R. A.; Lampe, K. J. Biomaterials via Peptide Assembly: Design, Characterization, and Application in Tissue Engineering. *Acta Biomater.* **2022**, *140*, 43–75. https://doi.org/10.1016/j.actbio.2021.10.030.

(22) Paramonov, S. E.; Jun, H.-W.; Hartgerink, J. D. Self-Assembly of Peptide−Amphiphile Nanofibers: The Roles of Hydrogen

Bonding and Amphiphilic Packing. *J. Am. Chem. Soc.* **2006**, *128* (22), 7291–7298. https://doi.org/10.1021/ja060573x.

(23) Worch, J. C.; Prydderch, H.; Jimaja, S.; Bexis, P.; Becker, M. L.; Dove, A. P. Stereochemical Enhancement of Polymer Properties. *Nat. Rev. Chem.* **2019**, *3* (9), 514–535. https://doi.org/10.1038/s41570-019-0117-z.

(24) Tsuji, H. Poly(Lactide) Stereocomplexes: Formation, Structure, Properties, Degradation, and Applications. *Macromol. Biosci.* **2005**, *5* (7), 569–597. https://doi.org/10.1002/mabi.200500062.

(25) Tsuji, H. Poly(Lactic Acid) Stereocomplexes: A Decade of Progress. *Adv. Drug Deliv. Rev.* **2016**, *107*, 97–135. https://doi.org/10.1016/j.addr.2016.04.017.

(26) Ren, J. M.; Lawrence, J.; Knight, A. S.; Abdilla, A.; Zerdan, R. B.; Levi, A. E.; Oschmann, B.; Gutekunst, W. R.; Lee, S.-H.; Li, Y.; McGrath, A. J.; Bates, C. M.; Qiao, G. G.; Hawker, C. J. Controlled Formation and Binding Selectivity of Discrete Oligo(Methyl Methacrylate) Stereocomplexes. *J. Am. Chem. Soc.* **2018**, *140* (5), 1945–1951. https://doi.org/10.1021/jacs.7b13095.

(27) Ren, J. M.; Knight, A. S.; van Ravensteijn, B. G. P.; Kohl, P.; Bou Zerdan, R.; Li, Y.; Lunn, D. J.; Abdilla, A.; Qiao, G. G.; Hawker, C. J. DNA-Inspired Strand-Exchange for Switchable PMMA-Based Supramolecular Morphologies. *J. Am. Chem. Soc.* **2019**, *141* (6), 2630–2635. https://doi.org/10.1021/jacs.8b12964.

(28) Abdilla, A.; Dolinski, N. D.; de Roos, P.; Ren, J. M.; van der Woude, E.; Seo, S. E.; Zayas, M. S.; Lawrence, J.; Read de Alaniz, J.; Hawker, C. J. Polymer Stereocomplexation as a Scalable Platform for Nanoparticle Assembly. *J. Am. Chem. Soc.* **2020**, *142* (4), 1667–1672. https://doi.org/10.1021/jacs.9b10156.

(29) Longo, J. M.; DiCiccio, A. M.; Coates, G. W. Poly(Propylene Succinate): A New Polymer Stereocomplex. *J. Am. Chem. Soc.* **2014**, *136* (45), 15897–15900. https://doi.org/10.1021/ja509440g.

(30) Auriemma, F.; De Rosa, C.; Di Caprio, M. R.; Di Girolamo, R.; Ellis, W. C.; Coates, G. W. Stereocomplexed Poly(Limonene Carbonate): A Unique Example of the Cocrystallization of Amorphous Enantiomeric Polymers. *Angew. Chem. Int. Ed.* **2015**, *54* (4), 1215–1218. https://doi.org/10.1002/anie.201410211.

(31) Auriemma, F.; De Rosa, C.; Di Caprio, M. R.; Di Girolamo, R.; Coates, G. W. Crystallization of Alternating Limonene Oxide/Carbon Dioxide Copolymers: Determination of the Crystal Structure of Stereocomplex Poly(Limonene Carbonate). *Macromolecules* **2015**, *48* (8), 2534–2550. https://doi.org/10.1021/acs.macromol.5b00157.

(32) de Jong, S. J.; van Eerdenbrugh, B.; van Nostrum, C. F.; Kettenes-van den Bosch, J. J.; Hennink, W. E. Physically Crosslinked Dextran Hydrogels by Stereocomplex Formation of Lactic Acid Oligomers: Degradation and Protein Release Behavior. *J. Controlled Release* **2001**, *71* (3), 261–275. https://doi.org/10.1016/S0168-3659(01)00228-0.

(33) Hennink, W. E.; De Jong, S. J.; Bos, G. W.; Veldhuis, T. F. J.; van Nostrum, C. F. Biodegradable Dextran Hydrogels Crosslinked by Stereocomplex Formation for the Controlled Release of Pharmaceutical Proteins. *Int. J. Pharm.* **2004**, *277* (1–2), 99–104. https://doi.org/10.1016/j.ijpharm.2003.02.002.

(34) Sun, L.; Pitto-Barry, A.; Kirby, N.; Schiller, T. L.; Sanchez, A. M.; Dyson, M. A.; Sloan, J.; Wilson, N. R.; O'Reilly, R. K.; Dove, A. P. Structural Reorganization of Cylindrical Nanoparticles Triggered by Polylactide Stereocomplexation. *Nat. Commun.* **2014**, *5* (1), 5746. https://doi.org/10.1038/ncomms6746.

(35) Nagy, K. J.; Giano, M. C.; Jin, A.; Pochan, D. J.; Schneider, J. P. Enhanced Mechanical Rigidity of Hydrogels Formed from Enantiomeric Peptide Assemblies. *J. Am. Chem. Soc.* **2011**, *133* (38), 14975–14977. https://doi.org/10.1021/ja206742m.

(36) Nagy-Smith, K.; Beltramo, P. J.; Moore, E.; Tycko, R.; Furst, E. M.; Schneider, J. P. Molecular, Local, and Network-Level Basis for the Enhanced Stiffness of Hydrogel Networks Formed from Coassembled Racemic Peptides: Predictions from Pauling and Corey. *ACS Cent. Sci.* **2017**, *3* (6), 586–597. https://doi.org/10.1021/acscentsci.7b00115.

(37) Raskatov, J. A.; Schneider, J. P.; Nilsson, B. L. Defining the Landscape of the Pauling-Corey Rippled Sheet: An Orphaned Motif Finding New Homes. *Acc. Chem. Res.* **2021**, *54* (10), 2488–2501. https://doi.org/10.1021/acs.accounts.1c00084.

(38) Swanekamp, R. J.; DiMaio, J. T. M.; Bowerman, C. J.; Nilsson, B. L. Coassembly of Enantiomeric Amphipathic Peptides into Amyloid-Inspired Rippled β-Sheet Fibrils. *J. Am. Chem. Soc.* **2012**, *134* (12), 5556–5559. https://doi.org/10.1021/ja301642c.

(39) Swanekamp, R. J.; Welch, J. J.; Nilsson, B. L. Proteolytic Stability of Amphipathic Peptide Hydrogels Composed of Self-Assembled Pleated β-Sheet or Coassembled Rippled β-Sheet Fibrils. *Chem Commun* **2014**, *50* (70), 10133–10136. https://doi.org/10.1039/C4CC04644G.

(40) Urban, J. M.; Ho, J.; Piester, G.; Fu, R.; Nilsson, B. L. Rippled β-Sheet Formation by an Amyloid-β Fragment Indicates Expanded Scope of Sequence Space for Enantiomeric β-Sheet Peptide Coassembly. *Molecules* **2019**, *24* (10), 1983. https://doi.org/10.3390/molecules24101983.

(41) Tang, J. D.; Mura, C.; Lampe, K. J. Stimuli-Responsive, Pentapeptide, Nanofiber Hydrogel for Tissue Engineering. *J. Am. Chem. Soc.* **2019**, *141* (12), 4886–4899. https://doi.org/10.1021/jacs.8b13363.

(42) Tang, J. D.; Roloson, E. B.; Amelung, C. D.; Lampe, K. J. Rapidly Assembling Pentapeptides for Injectable Delivery (RAPID) Hydrogels as Cytoprotective Cell Carriers. *ACS Biomater. Sci. Eng.* **2019**, *5* (5), 2117–2121. https://doi.org/10.1021/acsbiomaterials.9b00389.

(43) Duvaud, S.; Gabella, C.; Lisacek, F.; Stockinger, H.; Ioannidis, V.; Durinx, C. Expasy, the Swiss Bioinformatics Resource Portal, as Designed by Its Users. *Nucleic Acids Res.* **2021**, *49* (W1), W216–W227. https://doi.org/10.1093/nar/gkab225.

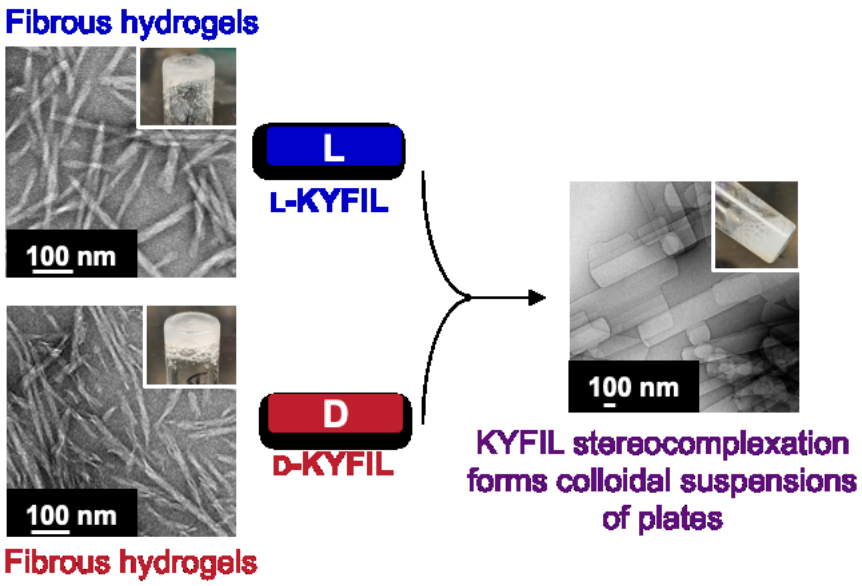
Fibrous hydrogels
100 nm
L
L-KYFIL
100 nm
D
D-KYFIL
Fibrous hydrogels
100 nm
KYFIL stereocomplexation forms colloidal suspensions of plates